Preprint typeset in JINST style - HYPER VERSION

In-situ calibration of the single-photoelectron charge response of the IceCube photomultipliers

IceCube author list to be inserted... E-mail: analyses@icecube.wisc.edu

ABSTRACT: This article outlines the in-situ calibration of the single-photoelectron charge distributions for each of the Hamamatsu Photonics R7081-02 photomultipliers in the IceCube Neutrino Observatory. The accurate characterization of the individual PMT charge distributions is important for event reconstruction and calibration. We discuss the single photoelectron identification procedure and how we extract the single-photoelectron charge distribution using a deconvolution of the multiple photoelectron charge distribution, and we examine various correlations between the shape of the single-photoelectron charge distribution and various hardware components. The time dependence of the charge distributions is also investigated.

Definitions (this will be removed in the final draft):

1. Charge: WaveDeform fits the waveform with an SPE pulses template. The integral of the fitted pulse, divided by the load resistance, divided by the gain, is the reported measured *charge* of the pulse. It is reported in units of a single electron.

2. PE: The unit of charge. This represents the charge relative to one electron.

3. 1 PE: The HV on each DOM is set such that the gain on the PMT is 10^7. It is determined to be at the proper gain (10^7), when the Gaussian mean of the fitted charge distribution is at 1 PE.

4. Photoelectron: The physical electron emitted from the photocathode.

5. SPE: (Single Photoelectron) A single physical electron emitted from the photocathode.

6. MPE: Multiple electrons emitted from the photocathode, charges may have been combined.

7. Charge distribution: The distribution of the measured charges. This will include both SPE and MPE events.

8. Single Photoelectron Charge distribution: The hypothetical charge distribution generated by observing a pure sample of single photoelectron.

9. SPE Template: The functional form that is used to fit the charge distribution.

KEYWORDS: IceCube, single photoelectron, charge distribution, PMT.

Contents

1. Introduction

The IceCube Neutrino Observatory [1, 2] is a cubic-kilometer-sized array of 5,160 photomultiplier tubes (PMTs) buried in the Antarctic ice sheet designed to observe high-energy neutrinos interacting with the ice [3]. In 2011, the IceCube Collaboration completed the installation of 86 vertical *strings* of PMT modules, eight of which were arranged in a denser array for the DeepCore detector [4] and the remaining for the main IceCube detector. Each string in the detector contains 60 digital optical modules (DOMs), which contain a single PMT each, as well as all required electronics [5]. The DOMs extend from 1450 m to 2450 m below the surface of the ice sheet and are spaced 17 m apart in the IceCube detector, and 7 m apart in the DeepCore detector.

Each DOM consists of a 0.5" thick spherical glass pressure vessel that houses a single downfacing 10" R7081-02 PMT from Hamamatsu Photonics [6]. The PMT is specified for wavelengths ranging from 300 nm to 650 nm, with peak quantum efficiency of 25% near 390 nm, classified as normal quantum efficiency (NQE) DOMs. Each PMT is coupled to the glass housing with optical gel and is surrounded by a wire mesh of μ metal to reduce the effect of the Earth's ambient magnetic field. The glass housing is transparent to wavelengths 350 nm and above [7].

IceCube has also deployed 399 DOMs with Hamamatsu R7081-02MOD PMTs, which, having a peak quantum efficiency of 34% near 390 nm (36% higher efficiency than the standard DOMs),

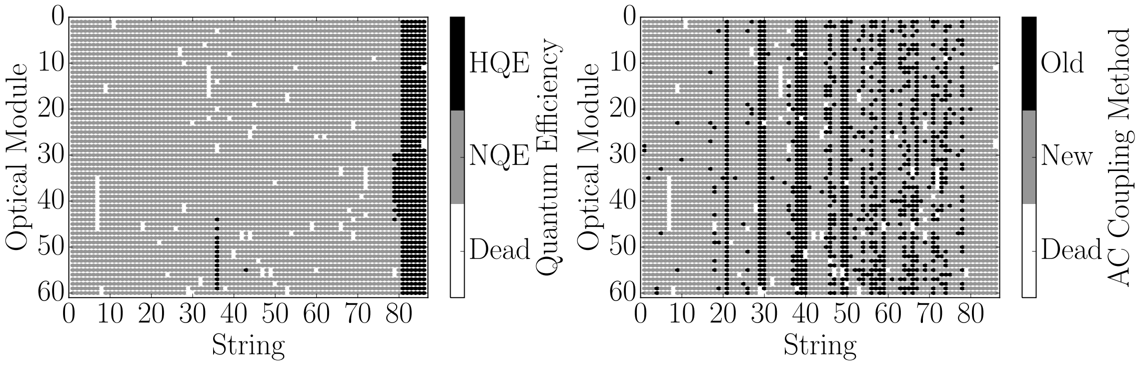

Figure 1. Left: A mapping of the HQE DOMs (black) and standard NQE DOMs (gray). Right: The version of AC coupling, old toroids (black) and new toroids (gray). DOMs that have been removed from service are shown in white.

are classified as high quantum efficiency (HQE) DOMs [4]. These DOMs are primarily located in DeepCore and on strings 36 and 43, as shown in the left side of Fig. 1.

The R7081-02 and R7081-02MOD PMTs have 10 dynode stages and are operated with a gain of 10^7 and high voltage around 1200 V (a typical amplified single photoelectron will generate a $\approx$6 mV peak voltage at the input to the front-end amplifiers). The PMTs operate with the anodes at high voltage and the signal is AC coupled to the front-end amplifiers. There are two versions of AC coupling in the detectors, both of which use custom-designed wideband bifilar wound 1:1 toroidal transformers[1] (the DOM-specific AC-coupling versions, new and old toroids, are shown on the right side of Fig. 1). The DOMs with the old toroids were designed with an impedance of 43Ω, while the new toroids are 50Ω [8].

IceCube relies on two observables per DOM to reconstruct events: the total number of detected photons and their timing distribution. Both the timing and the number of photons are extracted from the on-board digitized waveforms in software. The waveforms are deconvolved into a series of scaled single photoelectron pulses (so-called pulse series) and the integral of the individual pulses (divided by the load resistance) defines the observed charge. It will often be expressed in units of PE, or photoelectrons, which further divides the measured charge by the charge of a single electron times the nominal gain (10^7). Accurate characterization of the individual PMT charge distributions is crucial for calibration and event reconstructions relying on charge information. The charge distribution can also be used to assess long-term detector performance and identify discrepancies between data and Monte Carlo. It is therefore critically important to accurately measure the single-photoelectron (SPE) charge distribution in order to understand the IceCube detector behavior.

When one or more photons produce a voltage at the anode sufficient to trigger the onboard discriminator (set via a DAC to approximately 1.3 mV, or equivalently to 0.25PE), the signal acquisition process is triggered. The signal is fed into four parallel input channels. Three of the

[1] Conventional AC-coupling high-voltage ceramic capacitors can produce noise from leakage currents and impractical requirements on the capacitors in order to meet the signal droop and undershoot requirements. The toroidal transformer effectively acts as a high-pass filter with good signal fidelity at high frequencies. It also provides higher reliability than capacitive coupling and reduces the stored energy, which might cause damage if there is HV discharge in the system [7]. However, the toroidal-transformer AC coupling also introduces signal droop and undershoot.

channels pass first through a 75 ns delay loop in order to capture the leading edge of the pulse and then into three high-speed (300 MSPS for 128 samples) 10-bit waveform digitizers (Analog Transient Waveform Digitizer, ATWD), each of which has a different level of amplification (15.7 $\pm$ 0.6, 1.79 $\pm$ 0.06, and 0.21 $\pm$ 0.01 [8]). There are also three extra ATWDs on board each DOM: one is used for calibration and the other two operate in a ping-pong fashion to remove dead time associated with the readout. The signal to the fourth channel is first shaped and amplified and then fed into a 10-bit fast analog-to-digital converter (fADC) operating at a sampling speed of 40 MSPS. Further detail regarding the description of the DOM electronics can be found in Refs. [5, 9].

This article discusses the accurate determination of how individual DOMs collect charge in order to improve calibration and the detector description as used in the IceCube Monte Carlo simulation. It describes the procedure for determining the PMT's gain characteristics as seen in the SPE charge distributions using in-situ data from the IceCube and DeepCore detectors. The SPE charge distribution refers to the measured charge probability density function of the individual DOMs generated by the amplification of a pure sample of single photoelectrons. The extraction of the SPE charge distribution was recently made possible from the development of two pieces of software:

1. A specially-designed unbiased pulse selection was developed to reduce the multiple photoelectron (MPE) contamination while accounting for physical phenomena (e.g., late pulses, afterpulses, pre-pulses, and baseline shifts) and software-related effects (e.g., pulse splitting). This is further described in Sec. 2.1.

2. A fitting procedure was developed that separates the remaining MPE contamination from the SPE charge distribution by deconvolving the measured charged distribution. This is further described in Sec. 2.3.

By using in-situ data to determine the SPE charge distributions, we accurately represent the individual PMT response as a function of time, environmental conditions, software version, and hardware differences, and we sample photons uniformly over the surface of the photocathode. This is beneficial since it also allows us to inspect the stability and long-term behavior of the individual DOMs, verify previous calibration, and correlate features and environment to DOM behavior.

1.1 Single-photoelectron charge distributions

In an idealized scenario, a single photon produces a single photoelectron, which is then amplified by a known amount and the measured charge corresponds to 1 PE. However, there are many physical processes that create structure in the measured charge distributions. For example:

- **Statistical fluctuation due to cascade multiplication** [10]. At every stage of dynode amplification, there is a stochastic spread in the number of emitted electrons that make it to the next dynode. This in turn causes a spread in the measured charge after the gain stage of the PMT.

- **Photoelectron trajectory**. Some electrons may deviate from the favorable trajectory, reducing the number of secondaries produced at a dynode or the efficiency to collect them on the following dynode. This can occur at any stage, but it has the largest effect on the multiplication at the first dynode [11]. The trajectory of a photoelectron striking the first dynode will depend on many things, including where on the photocathode it was emitted, the uniformity of the electric field, the size and shape of the dynodes [10], and the ambient magnetic field [12, 13].

- **Late or delayed pulses**. A photoelectron can elastically or inelastically scatter off the first dynode. The scattered electron can then be re-accelerated to the dynode, creating a second pulse. The difference in time between the initial pulse and the re-accelerated pulse in the R7081-02 PMT was previously measured to be up to 70 ns [7, 14]. The two sub-pulses have lower charges, but the sum of the two tends to add up to the original charge. Collecting either the initial pulse or the late pulse will result in the charge being reconstructed in the low-PE region [15].

- **Afterpulses**. When a photoelectron or the secondary electrons produced during the electron cascade gain sufficient energy to ionize residual gas in the PMT, the positively charged ionized gas will be accelerated in the electric field towards the photocathode. Upon impact with the photocathode, electrons can be again released from the photocathode, creating what is called an afterpulse. For the R7081-02 PMTs, the timescale for afterpulses was measured to occur from 0.3 to 11 μs after the initial pulse, with the first prominent afterpulse peak occurring at approximately 600 ns [7]. The spread in the afterpulse time is dependent on the position of photocathode, the charge-to-mass ratio of the ion produced, and the electric potential distribution [16], whereas the size of the afterpulse is related to the momentum and species of the ionized gas and composition of the photocathode [17].

- **Pre-pulses**. If an incident photon passes through the photocathode without interaction and strikes one of the dynodes, it can eject an electron that is only amplified by the subsequent stages, resulting in a lower measured charge (lower by a factor of approximately 25). For the IceCube PMTs, the prepulses have been found to arrive approximately 30 ns before the signal from other photoelectrons from the photocathode [7].

- **MPE contamination**. When multiple photoelectrons arrive at the first dynodes within several nanoseconds of each other, they can be reconstructed by the software as a single, MPE pulse.

- **Electronic noise**. This refers to the fluctuations in the analog-to-digital converters (ATWDs and FADC) and ringing that arises from the electronics.

Beyond the physical phenomena above that modify the measured charge distribution, there is also a lower limit on the smallest charge that can be extracted. For IceCube, the discriminator limits the trigger pulse to be above approximately 0.25PE, and subsequent pulses in the readout time window are subject to a software-defined threshold. The software threshold was set conservatively to avoid extracting pulses that originated from electronic noise. This threshold can be modified to gain access to lower charge pulses and will be discussed in Sec. 2.2.

The standard charge distribution model used by the IceCube Collaboration (known as the TA0003 distribution [7]) represented the above effects as the sum of an exponential plus a Gaussian, where the exponential represented charge of poorly amplified pulses and the Gaussian represented the spread in statistical fluctuations due to the cascade multiplication. The TA0003 distribution was previously used to describe all the PMTs in the IceCube and DeepCore detectors.

Recently, IceCube has performed several lab measurements using the R7081-02 PMTs with in-time laser pulses, demonstrating that the in-time charge distribution includes a steeply falling low-charge component below the discriminator threshold. To account for this, a new functional form including a second exponential was introduced. This form of the charge distribution, $f(q)_{SPE} = Exp_1 + Exp_2 +$ Gaussian, is referred to as the *SPE template* in this article. Explicitly, it is:

$$f(q)_{SPE} = E_1 e^{-q/w_1} + E_2 e^{-q/w_2} + N e^{-\frac{(q-\mu)^2}{2\sigma^2}}, \tag{1.1}$$

where q represents the measured charge; E_1, E_2, and N represent normalization factors of each components; w_1 and w_2 are the exponential decay widths; and μ, σ are the Gaussian mean and width, respectively. This is the assumed functional shape of the SPE charge distributions and the components of Eq. 1.1 are determined in this article for all in-ice DOMs. IceCube defines 1 PE as the location of the Gaussian mean (μ) and calibrates the gain on the individual PMTs during the start of each season to meet this definition. The choice of where we define 1 PE is arbitrary, since linearity between the total charge collected to the number of incident photons is guaranteed. This is because the average of the distribution is a set fraction of the Gaussian mean and the mean of a N-fold convolution is the sum of means (central limit theorem). Any bias in the total observed charge can be absorbed into an efficiency term, such as the quantum efficiency.

1.2 IceCube datasets and software definitions

The largest contribution to the IceCube trigger rate comes from downgoing muons produced in cosmic ray induced showers [18]. Cosmic ray muons stopping in the detector cause the individual trigger rate to decrease at lower depths. Further, during the formation of this ice sheet, there have been several periods of colder climate that have caused the optical properties of the ice to differ at various depths. The optical properties also affect the trigger rate; in particular, the “dust layer" from 2100 to 2200 m below the surface (optical modules 32 to 38 in the IceCube detector) is a region in the ice with relatively large scattering and absorption coefficients [19].

An induced signal in the PMT that passes through the AC coupling toroid located on the base of the PMT is compared to a discriminator threshold. If two DOMs within two DOM distances of each other observe a passing of the discriminator, a *hard local coincidence* (HLC) is initiated and the corresponding waveforms are sampled 128 times and read out on the three ATWDs.

After waveform digitization, there is a correction applied to remove the measured DC baseline offset. The signal droop and undershoot introduced by the toroidal transformer AC coupling is compensated for in software (during waveform calibration) by adding the expected temperature-dependent reaction voltage of the undershoot to the calibrated waveform. If the undershoot voltage drops below 0 ADC counts, the ADC values are zeroed and then compensated for once the waveform is above the minimum ADC input. Scaled single photoelectron pulse shapes (that take into account the version of the AC coupling) are then fit to the waveforms using software referred to as WaveDeform (waveform unfolding process), which determines the individual pulse time stamps and charges and populates a pulse series [20].

The pulse series used in this analysis come from two datasets provided by IceCube:

1. The **MinBias dataset.** This dataset records the full waveform readout of randomly-triggered HLC events at a rate that corresponds on average to 1/1000 events. The largest contribution to the IceCube trigger rate comes from downgoing muons produced in cosmic-ray-induced showers [18] and therefore is the largest signal component in this dataset. These muons tend to have small energies when they reach the detector, thus they produce minimal MPE contamination. The full waveform of these events allows us to extract the raw information about the individual pulses. This will be used to measure the individual PMT charge distributions.

2. The **BeaconLaunch dataset.** This is a forced trigger (not triggered by the discriminator) filter that is typically used to monitor the individual DOM baseline. It includes the full ATWD-window waveform readout. Since this dataset is forced-triggered, the majority of these waveforms represent baseline fluctuations with minimal contamination from the occasional coincidental pulse that makes it into the readout window. This dataset will be used to examine the noise contribution to the charge distributions. Note: when using this dataset, the weight of every pulse is multiplied by a factor of 28.4 to account for the livetime difference between the MinBias dataset and the BeaconLaunch dataset. Weight, in this context, refers to the number of photons in the MinBias dataset proportional to one photon in the BeaconLaunch dataset for which both datasets have the same equivalent livetime.

This analysis uses the full MinBias and BeaconLaunch datasets from IceCube seasons 2011 to 2016 (subsequently referred to as IC86.2011 to IC86.2016). Seasons in IceCube typically start in June of the labeled year and end approximately one year later. Calibration is performed at the beginning of each season.

2. Extracting the SPE templates

2.1 Single photoelectron pulse selection

The pulse selection is the method used to extract candidate, unbiased, single photoelectron pulses from data while minimizing the MPE contamination. It avoids collecting afterpulses, rejects late pulses from the trigger, reassembles late pulses, accounts for the discriminator threshold, reduces the effect of droop and baseline undershoot, and gives sufficient statistics to perform a season-to-season measurement. An illustrative diagram of the pulse selection is shown in the left side of Fig. 2, while a description of the procedure is detailed below.

In order to trigger a DOM, the input to the front-end amplifiers must exceed the discriminator threshold. To avoid the selection bias of the discriminator trigger, we ignore the trigger pulse as well as the entire first 100 ns of the time window. Ignoring the first 100 ns has the added benefit of also removing late pulses that could be attributed to the triggering pulse. To ensure we are not accepting afterpulses into the selection, we also enforce the constraint that the pulse of interest (POI) is within the first 375 ns of the ATWD time window. This also allows us to examine the waveform up to 50 ns after the POI (the ATWD time window is $\approx$425 ns). In the vicinity of the POI, we check that WaveDeform did not reconstruct any pulses up to 50 ns prior to the POI, or 100 to 150 ns after the POI (the light gray region of Fig. 2 (left)). This latter constraint is to reduce the probability of accidentally splitting a late pulse in the summation window.

Restrictions are put on the full ATWD waveforms as well, so as to ensure that the trigger pulse does not exceed 10 mV (to reduce the effect of the subsequent baseline undershoot due to the AC coupling or other artifacts from large pulses), and a global constraint ensures that the time window cannot contain any waveform that exceeds 20 mV (recall that a properly amplified SPE pulse is ≈ 6 mV).

If a pulse is reconstructed between 100 and 375 ns after the time window is opened and the voltage criteria are met, it is accepted as a candidate photoelectron and several checks are performed on the waveform prior to and after the pulse. The first check is to ensure that the waveform is near the baseline just before the rising edge of the POI. This is accomplished by ensuring that the waveform does not exceed 1 mV, 50 to 20 ns prior to the POI, and eliminates cases where the POI is a late pulse. We also ensure the waveform returns to the baseline by checking that no ADC measurement exceeds 1 mV, 100 to 150 ns after the POI (these constraints are illustrated as the horizontal red dotted lines and black arrows in the left side of Fig. 2).

If all the above criteria are met, we sum the reconstructed charges from the POI time (given by WaveDeform) to +100 ns (the dark gray area in Fig. 2 (left)). This ensures that any nearby pulses are either fully separated or fully added. WaveDeform may occasionally split an SPE pulse into multiple smaller pulses, therefore it is always critical to perform a summation of the charge within a window. The 100 ns summation also means that the pulse selection will occasionally accept MPE events.

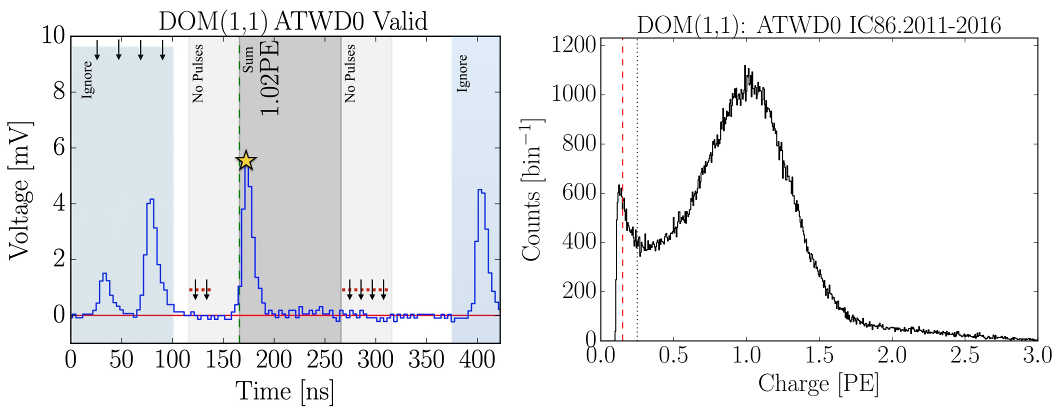

Figure 2. Left: An illustrative diagram of the pulse selection criteria for selecting a high-purity and unbiased sample of single photoelectrons. The digitized ATWD waveform is shown in blue. The pulse of interest is identified with a yellow star. This example waveform was triggered by a small pulse at 25 ns (recall that the delay board allows us to examine the waveform just prior to the trigger pulse), followed by a potential late pulse at 70 ns. At 400 ns, we see a pulse in the region susceptible to afterpulses. Waveform voltage checks are illustrated with arrows, and various time windows described in the text are drawn with semiopaque regions. The POI is reported to have a charge of 1.02 PE, given by WaveDeform, and would pass the pulse selection criteria. Right: The collected charges from string 1, optical module 1 (DOM 1,1), from the MinBias dataset collected from IC86.2011 to IC86.2016 that pass the pulse selection. The discriminator threshold at 0.25PE is represented as a dotted black vertical line. For visual purposes, a vertical dashed red line is also included at 0.15PE.

2.2 Characterizing the low-charge region

Fig. 2 (right) shows the charge distributions of the selected pulses that pass the single photoelectron pulse selection for string 1, optical module 1 (DOM (1,1)). In the low-charge region (below 0.25PE), we see a steep rise (in agreement with the in-time laser tests mentioned in Sec. 1.1), then a second threshold at approximately 0.13 PE. This is a software-defined threshold that comes from a gradient-related termination condition in WaveDeform. The threshold was set to avoid electronic noise being interpreted as PMT pulses and contaminating the low-charge region. This section will examine the effect on the charge distribution and noise contribution by lowering the WaveDeform threshold. The aim will be to explore the low-charge region.

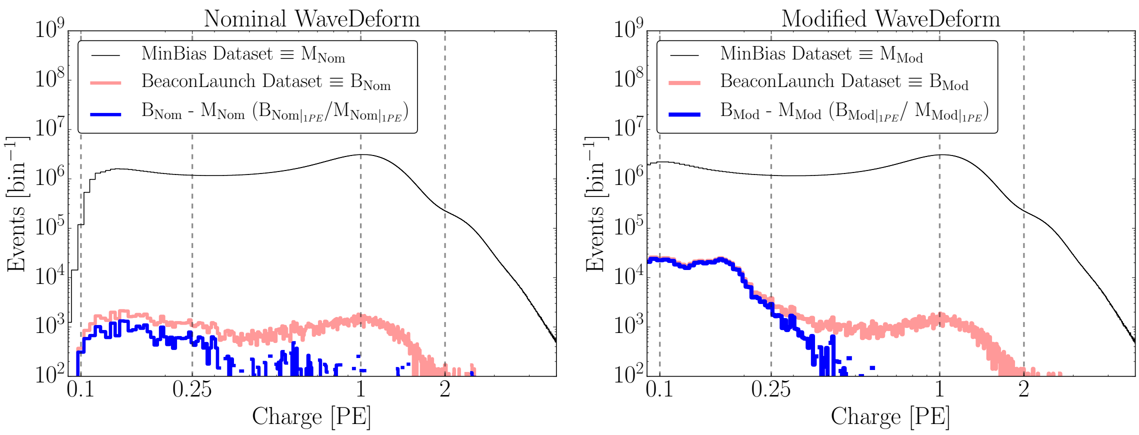

Figure 3. The cumulative charge distributions (IC86.2011 to 2016) of all DOMs for the MinBias and BeaconLaunch datasets. The blue histogram shows the expected contribution from noise (found by subtracting the shape of the MinBias dataset from the BeaconLaunch dataset). Left: The charge distributions for the standard WaveDeform settings. Right: The charge distributions for the modified WaveDeform settings.

Fig. 3 (left) shows the charge distributions for the MinBias (black) and the BeaconLaunch (red) datasets using the default settings of WaveDeform. As mentioned in Sec. 1.2, occasionally a photoelectron will be coincident with the forced BeaconLaunch time window. These charges populate a SPE distribution. Subtracting the shape of the MinBias charge distribution from the BeaconLaunch dataset yields an estimate of the amount of electronic noise contamination (blue). The bin with the largest signal-to-noise ratio (SNR) above 0.1 PE was found to have and SNR of 0.0013. The SNR for the full distribution was found to be 0.0005. Fig. 3 (right) shows the same data after lowering the WaveDeform threshold. Correspondingly, the bin with the largest SNR was found to be 0.0017, whereas the total SNR was found to be 0.0015.

2.3 Fitting procedure

The fit assumes that there is a negligible three-PE contribution, which is justified by the lack of statistics in the 3 PE region as well as the significant rate difference between the 1 PE and 2 PE region, as shown in Fig. 2 (right). The 2 PE charge distribution is assumed to be the SPE charge distribution convolved with itself [21]. A python-based piece of software called the "convolutional fitter" is used to determine the components of Eq. 1.1 from the measured charge distribution that includes the MPE contamination.

The Exp_2 component (as well as the Exp_1) of Eq. 1.1, represents poorly amplified photoelectrons, and we do not allow it to extend beyond the high-charge region of the Gaussian component. In particular, we include a constraint on the the parameter w_2 to ensure that it falls off with the Gaussian component:

$$w_2 < \frac{\mu + 2\sigma}{4 - \mathrm{Ln}(N/E_2)}. \tag{2.1}$$

This equation was found by setting the Exp_2 to be $1/e^2$ that of the Gaussian component at two sigma (the Exp_1 is neglected from this equation since it falls off in the low-charge region). Eq. 2.1 is used as a constraint during the fit to the charge distributions.

Pulses that fall below the WaveDeform threshold and are not reconstructed contribute to an effective efficiency of the individual DOMs. This analysis assumes the same shape of the steeply falling exponential component (Exp_1) for all DOMs in the detector to avoid large fluctuations in the individual DOM efficiencies. The modified WaveDeform data will strictly be used to determine the Exp_1 component. Specifically, using the modified WaveDeform, we will background-subtract the BeaconLaunch distribution from the MinBias data, fit the resulting distribution to determine the components of Eq. 2.1, and use only the measured shape and normalization of Exp_1 in all subsequent unmodified WaveDeform fits.

Upon fitting the MinBias data (with the predetermine values for Exp_1), the residual of each fit is calculated by measuring the percentage difference between the fit and the data. The average residual will then be used as a global scaling factor for all SPE templates to account for the difference between the chosen model (Eq. 2.1) and the actual data.

Failed fits (DOMs removed from service (109 DOMs) and DOMs that fail any one of several validity checks on the goodness of fit (6 DOMs)) are not included in this article. In the IceCube MC simulation chain, these DOMs are assigned the average SPE template.

2.4 SPE template fit results

Using the background-subtracted modified WaveDeform dataset, the steeply falling exponential component was determined by fitting the distribution from 0.1 PE to 3.5 PE to be $E_1 = 6.9 \pm 1.5$ and $w_1 = 0.032 \pm 0.002$ PE. The shape of the steeply falling exponential is then used to describe the low-PE charge region for all subsequent fits.

Using the MinBias dataset with the value for Exp_1 described above, the SPE templates are extracted for every DOM, separately for each IceCube season (IC86.2011 to IC86.2016). An average fit was also performed in which all the data for a given DOM was summed together (labeled as "AVG"). The fit range for

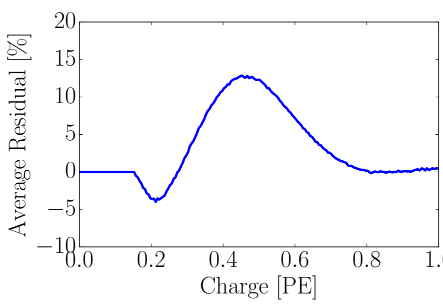

Figure 4. The measured average residual of the SPE templates fit.

Exp_2 and the Gaussian components are selected to be between 0.15 PE and 3.5 PE. The average residual for all DOMs from 0 to 1 PE is shown in Fig. 4.

An example fit is shown in Fig. 5 for the cumulative charge distribution for DOM (1,1). The collected charge distribution is shown in the black histogram, while the convolutional fit is shown as the black line (multiplied by the residual). The extracted SPE template (also multiplied by the residual) for this DOM is shown in blue.

The mean value and 1σ spread of the fit parameters, excluding Exp_1, for the IceCube and DeepCore detectors are shown in Table 1 and Table 2, respectively.

The individual DOM SPE templates were then examined between IceCube seasons for a time dependence of the fit parameters. For every DOM, the change over time of each fit parameter (excluding Exp_1) was calculated.

IceCube	Exp_2 Amplitude	Exp_2 Width	Gaus. Amplitude	Gaus. Mean	Gaus. Width
IC86.2011	0.601 ± 0.101	0.457 ± 0.070	0.736 ± 0.061	1.022 ± 0.030	0.296 ± 0.033
IC86.2012	0.595 ± 0.100	0.462 ± 0.065	0.740 ± 0.062	1.020 ± 0.034	0.295 ± 0.033
IC86.2013	0.602 ± 0.101	0.452 ± 0.071	0.736 ± 0.060	1.021 ± 0.033	0.298 ± 0.032
IC86.2014	0.597 ± 0.099	0.453 ± 0.071	0.736 ± 0.059	1.019 ± 0.030	0.299 ± 0.030
IC86.2015	0.604 ± 0.099	0.457 ± 0.067	0.735 ± 0.061	1.024 ± 0.032	0.296 ± 0.032
IC86.2016	0.600 ± 0.101	0.460 ± 0.063	0.736 ± 0.060	1.024 ± 0.030	0.295 ± 0.031

Table 1. The average values and 1σ spread of each fit parameter for the IceCube detector. The active DOMs in the IceCube detector are 99.4% NQE, and 31.0% of these DOMs have the old method of AC coupling. Correspondingly, there are 0.6% HQE DOMs, and 69.0% of these DOMs have the new version of AC coupling.

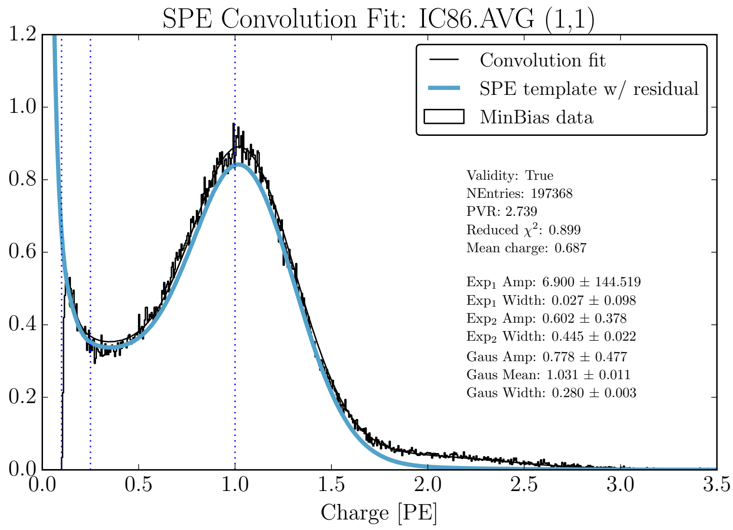

Figure 5. An example fit including the residual correction for DOM (1,1) using the WaveDeform dataset for seasons IC86.2011 to IC86.2016. The result from the convolutional fitter is shown as a solid black line. The extracted SPE template is shown blue.

DeepCore	Exp_2 Amplitude	Exp_2 Width	Gaus. Amplitude	Gaus. Mean	Gaus. Width
IC86.2011	0.519 ± 0.095	0.462 ± 0.099	0.763 ± 0.073	1.023 ± 0.031	0.307 ± 0.038
IC86.2012	0.517 ± 0.095	0.467 ± 0.098	0.763 ± 0.074	1.024 ± 0.032	0.306 ± 0.038
IC86.2013	0.520 ± 0.092	0.461 ± 0.096	0.763 ± 0.073	1.024 ± 0.030	0.306 ± 0.037
IC86.2014	0.522 ± 0.093	0.459 ± 0.098	0.765 ± 0.073	1.021 ± 0.031	0.306 ± 0.038
IC86.2015	0.525 ± 0.095	0.458 ± 0.099	0.763 ± 0.072	1.023 ± 0.031	0.307 ± 0.038
IC86.2016	0.522 ± 0.095	0.464 ± 0.098	0.763 ± 0.074	1.024 ± 0.031	0.305 ± 0.038

Table 2. The average values and 1σ spread of each fit parameter for the DeepCore detector. The active DOMs in DeepCore are 12.4% NQE, and 0.2% of these DOMs have the old method of AC coupling. Correspondingly, the DeepCore detector contains 87.6% HQE DOMs, and 99.8% of these DOMs have the new version of AC coupling.

Fig. 6 shows the change in a given fit parameter (represented as percentage deviation from the mean value), per year, of each DOM in both the IceCube (left) and DeepCore (right) detectors. The spread in the fit parameters was found to be consistent with statistically scrambling the yearly measurements. The average fit parameters are found to deviate less than 0.5% per year in both detectors, which is in agreement with the stability checks performed in Ref. [8].

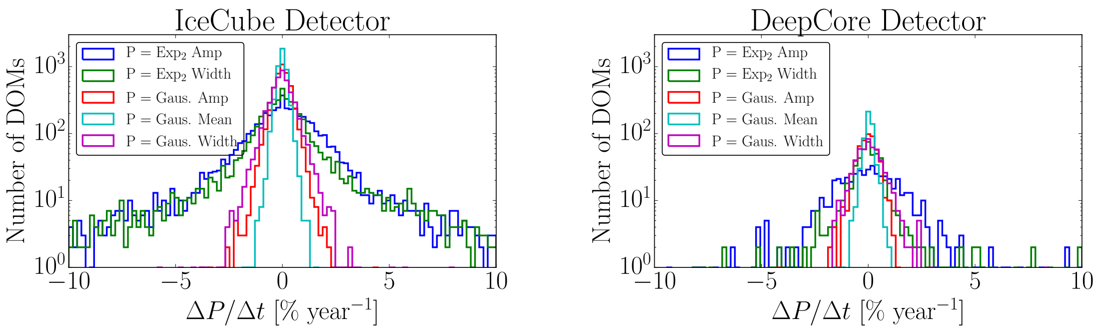

Figure 6. The change in individual DOM fitted parameters over time (Left: IceCube, Right: DeepCore). The change in the fit value is represented as percentage deviation from the mean fit parameter value.

3. Discussion

3.1 Correlations between fit parameters and DOM hardware differences

As noted in Sec. 1, there are two DOM-related hardware differences: the subset of HQE DOMs and the version of AC coupling used to couple the signal from the PMT anode to the front-end amplifiers. Correlations between the different hardware configurations were examined for correlations with the SPE template fit components.

The HQE DOMs were found to have a larger Exp_2 component (2.3% lower w_2 component and a 19.9% higher E_2, described in terms of Eq.1.1) than the standard DOMs[2]. Consequently, the HQE DOMs have a 14.9% lower peak-to-valley ratio and a 3.3% lower mean charge. These distributions are shown in Fig. 7. The change in the mean charge for the HQE DOMs is compensated for in

[2]This difference is still observed when comparing the DOMs at similar depths in the detector.

simulation by increasing the HQE DOM efficiency by the equivalent amount. This ensures that the total amount of charge collected by the HQE DOMs remains the same after the SPE templates are implemented.

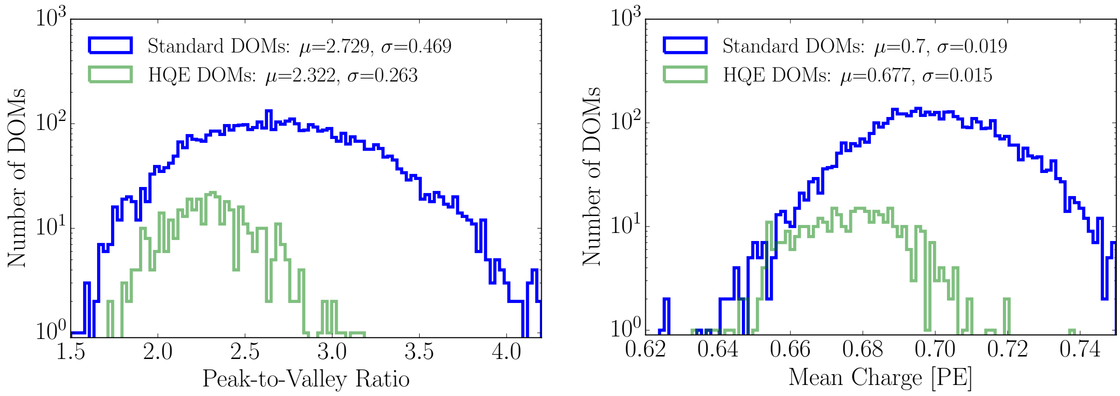

Figure 7. Comparison between the R7081-02MOD HQE DOMs and standard R7081-02 DOMs. Left: The peak-to-valley ratio for the two subsets of quantum efficiencies. Right: The mean charge of the individual DOM SPE templates.

The subset of NQE DOMs with the old AC coupling transformer was found to have a 6.1% narrower Gaussian width and an 8.0% larger Gaussian amplitude (σ and N in Eq. 1.1). The exponential component Exp_2 was also found to have a 7.5% lower E_2 component and a 3.0% higher E_2 component. Although the old toroid DOMs were deployed into the ice earlier than the new toroid DOMs, the difference above is still noted when examining individual deployment years; therefore, the shape differences are not attributed to the change in the DOM behavior over time. However, the DOMs with the old toroids used the first PMTs to be manufactured by Hamamatsu, so this difference may also be attributed to a gradual change in the process parameters over the course of PMT manufacturing, i.e., a change in the production procedure rather than the actual AC coupling version.

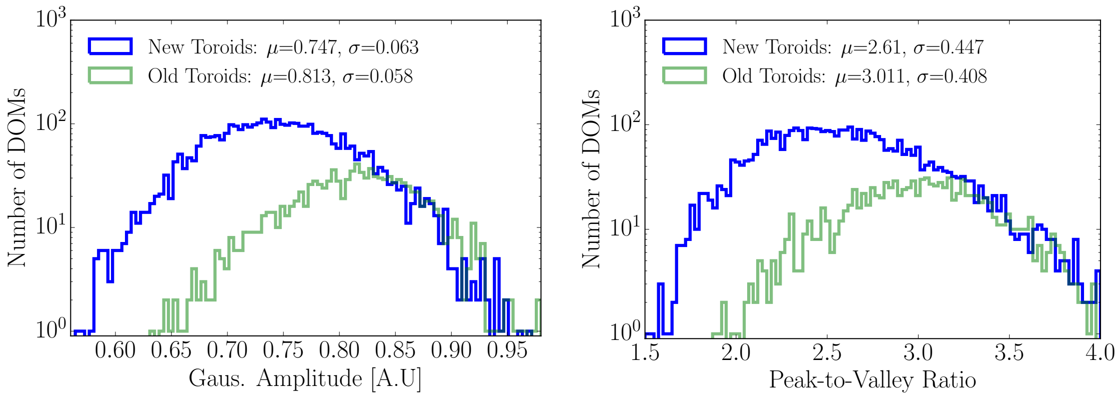

Figure 8. Comparison between the AC coupling versions used on the NQE DOMs. Left: The distribution of the measured Gaussian amplitudes. Right: The distribution of the measured peak-to-valley ratios.

3.2 Quantifying observable changes when modifying the PMT charge distributions

Changing the assumed gain response in simulation, as deduced from data, has different implications depending on the typical illumination level present in different analyses. These differences are outlined in the following discussion.

The PMT response is described by a combination of a "bare" efficiency, η_0, and a normalized charge response function, $f(q)$. The bare efficiency represents the fraction of arriving photons that result in any nonzero charge response, including those well below the discriminator threshold. The normalization condition is:

$$\int_0^{\inf} f(q)dq = 1. \tag{3.1}$$

Generally, $f(q)$ and η_0 have to be adjusted together to maintain agreement with a quantity known from lab or in-ice measurements, such as the predicted number of pulses above threshold for a dim source.

Dim source measurements Where light levels are low enough, subdiscriminator pulses do not contribute any observed charge because they do not satisfy the trigger threshold, and the probability of two photons arriving together is negligible. Given some independent way of knowing the number of arriving photons, a lab or in-ice measurement determines the trigger fraction above threshold $\eta_{0.25}$ and/or the average charge over threshold $Q_{0.25}$, either of which can be used to constrain the model as follows:

$$\eta_{0.25} = \eta_0 \int_{0.25q_{pk}}^{\inf} f(q)dq \tag{3.2}$$

$$Q_{0.25} = \eta_0 \int_{0.25q_{pk}}^{\inf} qf(q)dq \tag{3.3}$$

Here, the discriminator threshold is assumed to be 0.25 times the peak position q_{pk}. It is also useful to multiply observed charges by q_{pk}, since we set each PMT gain by such a reference, and then a measurement constraint would be stated in terms of $Q_{0.25}/q_{pk}$.

Semi-bright source measurements Once the ATWD window is open, subsequent pulses are not limited by the discriminator threshold. WaveDeform introduces a software termination condition at 0.1 PE (described at the end of Section 2.1). The average charge of an individual pulse that arrives within the time window is:

$$Q_{0.10} = \eta_0 \int_{0.10q_{pk}}^{\inf} qf(q)dq \tag{3.4}$$

Bright source measurements For light levels that are large, the trigger is satisfied regardless of the response to individual photons, and the total charge per arriving photon therefore includes contributions below both the discriminator and the WaveDeform thresholds:

$$Q_0 = \eta_0 \int_0^{\inf} qf(q)dq \tag{3.5}$$

As such, the total charge is directly proportional to the average charge of the SPE template, having a strong dependence on the steeply falling exponential.

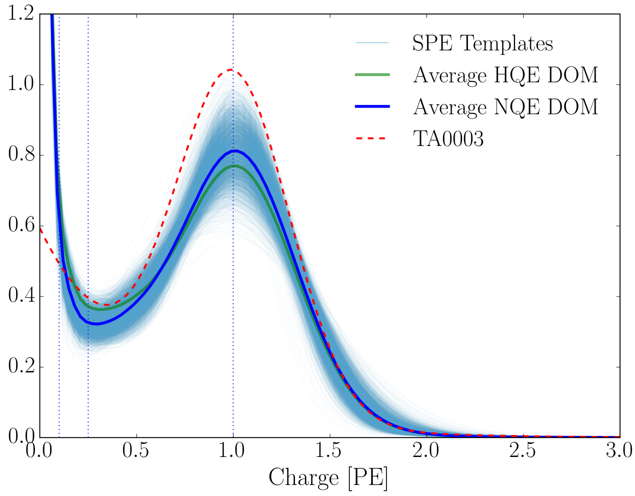

Figure 9. A comparison between the SPE templates (light blue band) and the TA0003 (dashed red line) distribution. The average SPE template for the NQE and HQE DOMs is shown as the thick blue and green lines, respectively. The SPE templates include the residual correction, and all curves are normalized.

3.2.1 Model comparison

When the charge distribution model is changed in a way that preserves agreement with the measured $\eta_{0.25}$ or $Q_{0.25}/q_{pk}$, i.e., η_0 is adjusted properly for changes in $f(q)$, the physical effect can be summarized by the change in the bright-to-dim ratios $Q_0/Q_{0.25}$, and $Q_0/Q_{0.10}$. Conveniently, these ratios depend only on the shape of $f(q)$. Table 3 compares these ratios in terms of the previous charge distribution (TA0003) and the SPE templates described here. It is shown that there are percent level differences in the physically-observable bright-to-dim ratios.

Model	Detector	$Q_0/Q_{0.25}$	$Q_0/Q_{0.10}$	$\eta_{0.25}/Q_{0.25}$
TA0003	IceCube and DeepCore	1.017	1.003	0.969
SPE Templates	IceCube	1.031±0.003	1.013±0.001	0.971±0.006
SPE Templates	DeepCore	1.034±0.002	1.014±0.001	0.965±0.006

Table 3. The distribution in bright-to-dim ratios for the previous charge distribution (TA0003) and the individual DOM SPE templates for the IceCube and DeepCore detectors.

Fig. 9 shows the shape difference between the TA0003 distribution and all the SPE templates measured in this article. The shape difference is attributed to better control of the low-charge region, the difference in functional form (described in Section 1.1), and the fact that the SPE templates sample uniformly over the entire photocathode at random incident angles. We have also separated the DOMs into the subsets of NQE and HQE DOMs to illustrate their average shape differences.

3.3 SPE templates in simulation

The IceCube Monte Carlo simulation chain assigns a charge to every photoelectron generated at the surface of the photocathode. The charge is determined by sampling from a normalized charge distribution probability density function. A comparison between describing the charge distribution using the SPE templates and the TA0003 distribution follows.

Two simulation sets consisting of the same events were processed through the IceCube Monte Carlo simulation chain to the final level of the multiyear high-energy sterile analysis. At analysis level, the events that pass the cuts are >99.9% pure upgoing (directed upwards relative to the horizon) secondary muons produced by charged current muon neutrino/antineutrino interactions. The muon energy range of this event selection is between 500 GeV and 10 TeV (reconstructed quantities).

Fig. 10 (left) shows the distribution of the total measured charge in a single DOM during each event. The data is shown for the full IC86.2012 season but is statistically equivalent to any of the other seasons. The simulation set using the TA0003 charge distribution is shown in orange, and that using the SPE templates is shown in blue. The bottom of the plot shows the ratio of the measured quantity relative to data. Fig. 10 (right) shows the distribution of the measured total charge on a DOM (after noise removal) divided by the number of channels, or DOMs, that participated in the event. Both plots in Fig. 10 have been normalized such that the area under the histograms is the same.

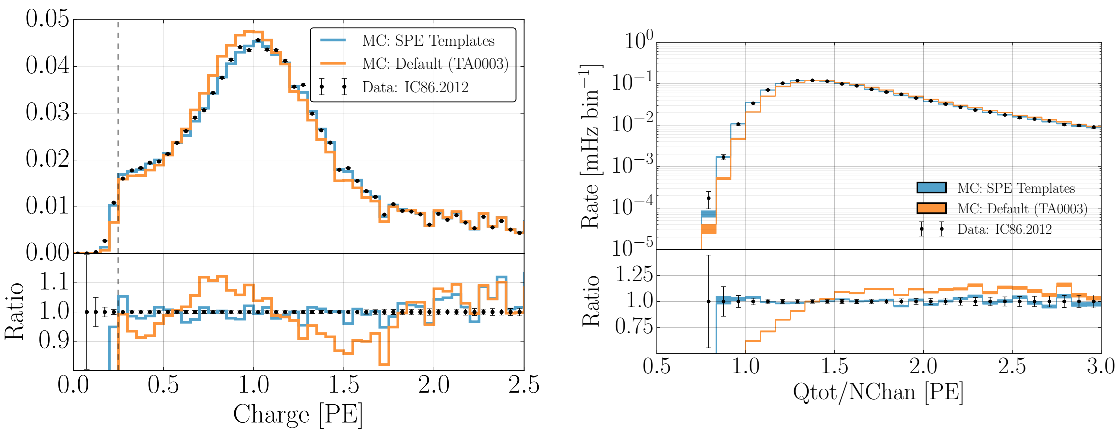

Figure 10. A comparison between the SPE templates (blue) and the TA0003 (orange) model for describing the SPE charge distribution in Monte Carlo. The simulation is compared to the 2012 IceCube season. Left: The total measured charge per DOM, per event at analysis level. Right: The distribution of the total measured charge of an event divided by the number of DOMs that participated in the event.

The SPE templates clearly improve the overall MC description of these two variables. IceCube includes a systematic uncertainty in all analyses, which scales the DOM efficiency to account for effects that change the total observed charge. This systematic compensates for the overall mean charge shift introduced using the SPE templates; however, the SPE templates now introduce DOM-to-DOM differences. This is not expected to change the IceCube physics results since analyses are sensitive to the overall detector performance rather than the individual DOM variations.

3.4 SPE templates for calibration

The gain setting on each DOM is calibrated at the beginning of the season such that the Gaussian mean charge distribution corresponds to a gain of 10^7 (equivalently labelled as 1 PE). Since the method used to extract the Gaussian mean described in this article is different from the previous method used for calibration of the DOMs, the total measured charge from a DOM is expected to change with the updated calibration.

As shown in Tables 1 and 2, the Gaussian mean component of the fit of every year is found to be on average 2.2% higher than unity, corresponding to a systematic overestimation of the measured charge in the detector. This correction to the measured charge can be implemented retroactively by dividing the reported charge from WaveDeform by the corresponding Gaussian mean for a given DOM. Alternatively, the MC can account for this difference by simply inserting the SPE templates with Gaussian mean matching the values found in the data. Both of these solutions will be used in future IceCube data/MC production.

4. Conclusion

This article outlines the procedure used for collecting a relatively pure sample of single photoelectron charges for each of the in-ice DOMs in IceCube. MPE contamination was removed under the assumption that it is the convolution of the SPE distribution from multiple times.

The SPE templates were extracted for each DOM and each season in the IceCube and DeepCore detectors and investigated for correlations with hardware-related features. Neither detector shows more than a 0.5% deviation in any of the fitted parameters over the investigated seasons, in agreement with Ref. [8]. Yearly variations in the fit parameters are consistent with statistical fluctuations. The HQE DOMs located in the IceCube and DeepCore detectors were found to have an Exp_2 component distinguishable from the standard DOMs. Similarly, DOMs with the old method of AC coupling were found to have a narrower and larger Gaussian component. This was not found to be due to a manufacturing process and is still under investigation.

The SPE templates were introduced into the MC simulation production and the result was compared to the default charge distribution. A significant improvement in the description of the low-level variables, total charge per DOM, and total charge per event over the number of channels was shown. IceCube includes a systematic that scales the bare efficiency of the DOMs to maintain agreement with a quantity known from lab or in-ice measurements. After accounting for this shift, the effect on physics analysis, as shown by the bright-to-dim ratios, is expected to be minimal (percent level changes in the measured charge).

The new method for extracting the calibration constant that determines the gain setting on each of the PMTs (the Gaussian mean of the fit) has been revised and shows that the average gain was approximately 2.2%$\pm$3.1% higher than expected. This will be implemented in future IceCube data reprocessing.

Acknowledgments

We acknowledge the support from the following agencies: U.S. National Science Foundation - Office of Polar Programs, U.S. National Science Foundation - Physics Division, University of Wisconsin Alumni Research Foundation, the Grid Laboratory Of Wisconsin (GLOW) grid infrastructure at the University of Wisconsin - Madison, the Open Science Grid (OSG) grid infrastructure; U.S. Department of Energy, and National Energy Research Scientific Computing Center, the Louisiana Optical Network Initiative (LONI) grid computing resources; Natural Sciences and Engineering Research Council of Canada, WestGrid and Compute/Calcul Canada; Swedish Research Council, Swedish Polar Research Secretariat, Swedish National Infrastructure for Computing (SNIC), and Knut and Alice Wallenberg Foundation, Sweden; German Ministry for Education and Research (BMBF), Deutsche Forschungsgemeinschaft (DFG), Helmholtz Alliance for Astroparticle Physics (HAP), Research Department of Plasmas with Complex Interactions (Bochum), Germany; Fund for Scientific Research (FNRS-FWO), FWO Odysseus programme, Flanders Institute to encourage scientific and technological research in industry (IWT), Belgian Federal Science Policy Office (Belspo); University of Oxford, United Kingdom; Marsden Fund, New Zealand; Australian Research Council; Japan Society for Promotion of Science (JSPS); the Swiss National Science Foundation (SNSF), Switzerland; National Research Foundation of Korea (NRF); Villum Fonden, Danish National Research Foundation (DNRF), Denmark.

References

[1] J. Ahrens *et al.*, "Icecube preliminary design document," *URL: http://www. icecube. wisc. edu/science/publications/pdd*, 2001.

[2] A. Achterberg, M. Ackermann, J. Adams, J. Ahrens, K. Andeen, D. Atlee, J. Baccus, J. Bahcall, X. Bai, B. Baret, *et al.*, "First year performance of the icecube neutrino telescope," *Astroparticle Physics*, vol. 26, no. 3, pp. 155–173, 2006.

[3] I. Collaboration *et al.*, "Evidence for high-energy extraterrestrial neutrinos at the icecube detector," *Science*, vol. 342, no. 6161, p. 1242856, 2013.

[4] R. Abbasi, Y. Abdou, T. Abu-Zayyad, M. Ackermann, J. Adams, J. Aguilar, M. Ahlers, M. Allen, D. Altmann, K. Andeen, *et al.*, "The design and performance of icecube deepcore," *Astroparticle physics*, vol. 35, no. 10, pp. 615–624, 2012.

[5] R. Abbasi, M. Ackermann, J. Adams, M. Ahlers, J. Ahrens, K. Andeen, J. Auffenberg, X. Bai, M. Baker, S. Barwick, *et al.*, "The icecube data acquisition system: Signal capture, digitization, and timestamping," *Nuclear Instruments and Methods in Physics Research Section A: Accelerators, Spectrometers, Detectors and Associated Equipment*, vol. 601, no. 3, pp. 294–316, 2009.

[6] Hamamatsu, "Datasheet," *URL: https://www.hamamatsu.com/*, 2018.

[7] R. Abbasi, Y. Abdou, T. Abu-Zayyad, J. Adams, J. Aguilar, M. Ahlers, K. Andeen, J. Auffenberg, X. Bai, M. Baker, *et al.*, "Calibration and characterization of the icecube photomultiplier tube," *Nuclear Instruments and Methods in Physics Research Section A: Accelerators, Spectrometers, Detectors and Associated Equipment*, vol. 618, no. 1-3, pp. 139–152, 2010.

[8] M. Aartsen *et al.*, "The icecube neutrino observatory: Instrumentation and online systems, jinst 12 (03)(2017) p03012," *arXiv preprint arXiv:1612.05093*, pp. 1748–0221.

[9] R. Stokstad, "Design and performance of the icecube electronics," 2005.

[10] Hamamatsu, "Resources: Basics and applications," *URL: https://www.hamamatsu.com/resources/pdf/etd/PMT_handbook_v3aE.pdf*, 2018.

[11] Hamamatsu, "Handbook resources, chapter 4," *URL: https://www.hamamatsu.com/resources/pdf/etd/PMT_handbook_v3aE-Chapter4.pdf*, 2018.

[12] J. Brack, B. Delgado, J. Dhooghe, J. Felde, B. Gookin, S. Grullon, J. Klein, R. Knapik, A. LaTorre, S. Seibert, *et al.*, "Characterization of the hamamatsu r11780 12 in. photomultiplier tube," *Nuclear Instruments and Methods in Physics Research Section A: Accelerators, Spectrometers, Detectors and Associated Equipment*, vol. 712, pp. 162–173, 2013.

[13] E. Calvo, M. Cerrada, C. Fernández-Bedoya, I. Gil-Botella, C. Palomares, I. Rodríguez, F. Toral, and A. Verdugo, "Characterization of large-area photomultipliers under low magnetic fields: Design and performance of the magnetic shielding for the double chooz neutrino experiment," *Nuclear Instruments and Methods in Physics Research Section A: Accelerators, Spectrometers, Detectors and Associated Equipment*, vol. 621, no. 1-3, pp. 222–230, 2010.

[14] F. Kaether and C. Langbrandtner, "Transit time and charge correlations of single photoelectron events in r7081 photomultiplier tubes," *Journal of Instrumentation*, vol. 7, no. 09, p. P09002, 2012.

[15] B. Lubsandorzhiev, P. Pokhil, R. Vasiljev, and A. Wright, "Studies of prepulses and late pulses in the 8" electron tubes series of photomultipliers," *Nuclear Instruments and Methods in Physics Research Section A: Accelerators, Spectrometers, Detectors and Associated Equipment*, vol. 442, no. 1-3, pp. 452–458, 2000.

[16] K. Ma, W. Kang, J. Ahn, S. Choi, Y. Choi, M. Hwang, J. Jang, E. Jeon, K. Joo, H. Kim, *et al.*, "Time and amplitude of afterpulse measured with a large size photomultiplier tube," *Nuclear Instruments and Methods in Physics Research Section A: Accelerators, Spectrometers, Detectors and Associated Equipment*, vol. 629, no. 1, pp. 93–100, 2011.

[17] S. Torre, T. Antonioli, and P. Benetti, "Study of afterpulse effects in photomultipliers," *Review of scientific instruments*, vol. 54, no. 12, pp. 1777–1780, 1983.

[18] M. Aartsen, K. Abraham, M. Ackermann, J. Adams, J. Aguilar, M. Ahlers, M. Ahrens, D. Altmann, T. Anderson, M. Archinger, *et al.*, "Characterization of the atmospheric muon flux in icecube," *Astroparticle physics*, vol. 78, pp. 1–27, 2016.

[19] M. Aartsen, R. Abbasi, Y. Abdou, M. Ackermann, J. Adams, J. Aguilar, M. Ahlers, D. Altmann, J. Auffenberg, X. Bai, *et al.*, "Measurement of south pole ice transparency with the icecube led calibration system," *Nuclear Instruments and Methods in Physics Research Section A: Accelerators, Spectrometers, Detectors and Associated Equipment*, vol. 711, pp. 73–89, 2013.

[20] M. Aartsen, R. Abbasi, M. Ackermann, J. Adams, J. Aguilar, M. Ahlers, D. Altmann, C. Arguelles, J. Auffenberg, X. Bai, *et al.*, "Energy reconstruction methods in the icecube neutrino telescope," *Journal of Instrumentation*, vol. 9, no. 03, p. P03009, 2014.

[21] R. Dossi, A. Ianni, G. Ranucci, and O. J. Smirnov, "Methods for precise photoelectron counting with photomultipliers," *Nuclear Instruments and Methods in Physics Research Section A: Accelerators, Spectrometers, Detectors and Associated Equipment*, vol. 451, no. 3, pp. 623–637, 2000.